Journal of Nondestructive Evaluation, Vol. 25, No. 3, September 2006 (© 2006)
DOI: 10.1007/s10921-006-0008-3

Considerations in the Validation and Application of Models for Eddy Current Inspection of Cracks Around Fastener Holes

Jeremy S. Knopp,[1,4] John. C. Aldrin,[2] and Pradeep Misra[3]

Received 22/09/2005; revised 30/06/2006; Published online: 30/9/2006

To improve the detection and characterization of cracks around fastener holes in multilayer structures without removing the fastener, model-based approaches are proposed to support the design of advanced eddy current (EC) NDE systems. This work demonstrates the validation and application of models to simulate EC inspection as part of the design process. The volume integral method (VIM) and finite element method (FEM) are both used to simulate eddy current inspection of fastener sites for fatigue cracks. Convergence studies, validation with existing models, experimental validation studies and validation through inverse method demonstrations are presented, providing a continuum of methods to ensure the quality of measurement models. Consideration concerning convergence and validation is also given with features sensitive to the sample geometry and flaw characteristics. A novel calibration technique is also presented to practically evaluate the transformation between model-based impedance calculations and experimental voltage data. A series of studies are presented concerning the detection of cracks around fastener holes demonstrating the quality of the simulated data to represent experimental measurements.

KEY WORDS: Eddy current; cracks; modeling; model validation; model convergence.

1. INTRODUCTION

The development of new inspection techniques for aging aircraft structures is a challenge when considering the need to detect widespread fatigue and corrosion damage in components not designed for inspection. In particular, there is a need to reliably detect cracks around fastener holes in multilayer structures without removing the fastener. A diagram of a typical fastener hole inspection problem is shown in Fig. 1. Ultrasonic and eddy current techniques are frequently employed to satisfy inspection requirements. In cases where the sealant between the layers is not present or known to be poor, ultrasonic techniques are unable to interrogate subsurface layers since there is no medium present for wave propagation. This work focuses on eddy current techniques which are appropriate when the total thickness of the structure is thin, usually less than half of an inch. Due to the nature of the physics, eddy current does not depend on the sealant conditions for penetration. When using eddy current, there are 3 primary challenges: 1) the penetration depth of the induced currents is limited by the skin depth, which makes the detection and resolution of defects more difficult as the depth increases, 2) there are tens of thousands of fastener hole sites that need to be inspected in a timely manner, 3) there are a number of irregular geometric factors such as misdrilled holes, varying contact or sealant conditions between the fastener and the hole,

[1] Metals, Ceramics, and NDE Division, Air Force Research Laboratory (AFRL/MLLP), Wright-Patterson AFB, OH 45433, USA.
[2] Computational Tools, Gurnee, IL 60031, USA.
[3] Department of Electrical Engineering, Wright State University, Dayton, OH 45435, USA.
[4] Corresponding author: E-mail: jeremy.knopp@wpafb.af.mil

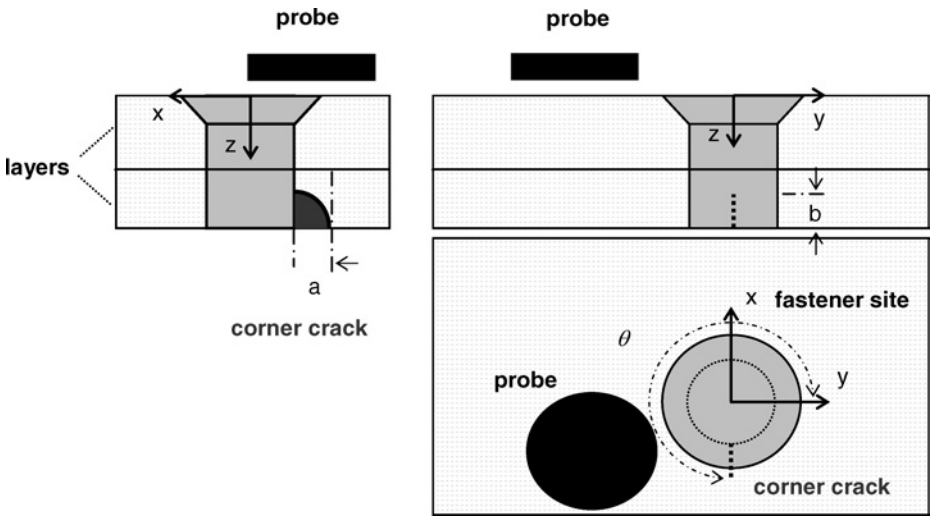

Fig. 1. Two-layer aircraft structure with corner crack emanating from a fastener hole in the second layer.

and unknown subsurface structures that are at least in part the cause of false calls and thus limit detection capability.

In addition to commercial inspection systems,[1,2] there is ongoing basic research in the area of probe design, sensor arrays, and signal processing. In recent work, a D-shaped coil was used to focus the incident field in order to maximize sensitivity around the fastener.[3] Another way to achieve a more focused incident field is to alter the geometry of the ferrite core.[3–5] In the past, non-axisymmetric segmented ferrite cores were shown to increase the eddy current densities in the vicinity of the crack location. Sensors that respond directly to the magnetic field as opposed to the receiver coils based on induction are increasingly being used. This provides a better frequency response, especially at low frequencies. Giant magnetoresistive (GMR), AMR, and Hall effect sensors have all been investigated for use in eddy current inspection systems.[6–10] To address the issue of inspection time, arrays of sensors are also being investigated and developed to inspect larger areas with reduced scan time.[11]

Models of nondestructive inspections offer many advantages to the NDE community. Potential applications for models in NDE system design include selection of NDE method, optimization of probe design and scan plans, reduction in the number of samples required for parametric studies, model-assisted probability of detection (MAPOD), implementation of model-based inverse methods for practical applications, and demonstration for training purposes. Previous work has benefited from the use of models for eddy current system design. Beissner et al used finite element method (FEM) models to study the effect of the geometry of the ferrite core in an eddy current probe. The studies indicated that a segmented ferrite core could actually focus the magnetic field in a way that allowed deeper defects to be detected.[5] Thollon et al used FEM models to optimize the excitation coil of an eddy current probe.[12] Wincheski et al also employed FEM models to study the induced eddy current densities as a function of a flux focusing lens thickness.[13] Nakagawa has developed an efficient computational software package based on the boundary element method to simulate bolt-hole inspections for cracks and study corner cracks.[14,15] The interest in model-assisted POD has increased considerably in recent years.[16] Examples for this particular application can be found in prior work.[17–19]

In order to increase the acceptance of models in the wider NDE community, rigorous methodologies for validation and application are needed. With the goal to apply models to problems of increasing complexity, the challenge remains to validate model accuracy and address any discrepancies between experiment and simulation that can hinder their application. To address this goal, convergence studies, validation with existing models, experimental validation studies and validation through inverse method demonstrations are presented, providing a continuum of methods to ensure the quality of measurement models. Consideration concerning convergence

and validation is also given with respect to features sensitive to the sample geometry and flaw characteristics. A novel calibration technique is also presented to practically evaluate the transformation between model-based impedance calculations and experimental voltage data, providing an efficient approach utilizing only a single calibration experiment. The quantitative basis for the validity of this approach is presented in this paper. Lastly, for the case study problem concerning the detection of cracks around fastener holes, excellent agreement was found between experimental and simulated data produced using both the volume integral method (VIM) and FEM.

2. MODELS AND CONVERGENCE

2.1. Modeling Approaches for the Case Study Problem

The volume integral method and finite element method were used to simulate eddy current phenomena for the generic inspection geometry shown in Fig. 1. VIC-3D®(V3.0), based on a volume integral formulation, was used to solve the electromagnetic scattering problem.[21–24] In this formulation, a flaw region is modeled as a fictitious current source, which is directly related to departures in electrical conductivity and magnetic permeability in the host material. Green's functions for infinitesimal current sources in multi-layered materials have been developed in previous work.[25–28] The method of moments is used to solve the volume integral equation.[29] The advantage of this formulation is that only the region of the scatterer needs to be discretized. In particular, the grid is regular in all 3 dimensions. Once the grid is introduced, the unknown current is expanded in terms of suitable 'bounded-divergence' functions, which are then used to test the equations, in the terminology of the Galerkin variant of the method-of-moments. Because of the regular grid, the resulting matrix has a very nice structure, being Toeplitz (convolutional) and Hankel (correlational), where very large problems can be solved efficiently using the conjugate-gradient method. In this or other iterative methods, the vector-matrix products can be rapidly calculated using three-dimensional Fast-Fourier Transforms (FFT).

The FEM model implemented in Opera-3D®software package (V9.0) was also used to simulate eddy current inspection of the case study problem.[30] The numerical formulation of FEM is well established in the literature[31,32]. Irregular meshes of tetrahedral elements were used with the finite element formulation to generally represent complex geometries. The output of this model is the electric and magnetic field intensities. Advantages of the model include the fact that the solution is valid and available in the entire domain and the ability to model awkward geometries.

The measurement model for an eddy current coil can be expressed in terms of changes in resistance and inductance

$$Z = R + j\omega L. \tag{1}$$

For a coil above a conductor, the change in resistance is associated with dissipated energy, P, in the region of the conductor, and is given by

$$R = \frac{P}{I^2}, \tag{2}$$

and the change in inductance corresponding with the stored energy, W, in the whole solution domain, Γ, is given by

$$L = \frac{2W}{I^2}. \tag{3}$$

Using the finite element solution for the electric and magnetic field intensities in the solution domain, the dissipated energy in the conductor (Γ') and stored energy in the whole solution domain (Γ) can be calculated as follows:

$$P = \int J^e E^* d\Gamma' \tag{4}$$

$$W = \frac{1}{2}\int HB^* d\Gamma. \tag{5}$$

To evaluate the change in impedance in a conductor due solely to the presence of a fastener and radial crack, the difference in impedance must be calculated from two separate problems representing 1) a pristine sample and 2) a sample containing a fastener and crack.

2.2. Model Convergence Studies

Convergence is a property of a numerical model that can be used to demonstrate model accuracy for a prescribed set of conditions associated with the sample geometry and material condition. Theoretically for both the VIM and FEM, as the dimensions of

the elements become small, the numerical simulation will approach the exact solution for the problem. Although not insured to accurately represent all details of an experiment measurement, especially for parameters that have not been properly considered in the model design, convergence studies do provide a form of validation of model accuracy for those conditions included in the model.

In this study, the volume integral method was chosen to demonstrate the benefits of convergence studies in support of model validation. In particular, VIM was used because meshing is limited only to 'flaw' regions (including the hole and crack geometry), meshes are regular in all three dimensions, and solution time is low. The case study problem (presented in prior work[33] and Section 4.1) including sample geometry, flaw dimensions, probe properties and frequency (set to 5.0 kHz) was used as the basis for the convergence study. An approximate probe model (neglecting the ferrite cup-core) was used to reduce model solution time which was especially beneficial for the high level of discretization used in the convergence study.

In the first series of studies, the number of elements along the x and y axis, N, was simultaneously ranged from 2 to 256 with increments of the power of 2. Given a diameter of the hole of 8.00 mm and the length of an EDM notch of 2.27 mm, the corresponding dimensions of the regular mesh region are 10.27 mm and 8.00 mm in the x and y directions respectively. For z axis discretization, the number of elements was fixed at 2. Figure 2(a) displays the simulated magnitude response as a function of x-axis scan position for varying the number of elements in the x and y directions for the case study problem demonstrating how the models approach a solution as the number of elements are increased. To better quantify the degree to which these numerical solutions approach an 'exact' solution, an error analysis of the data was performed. For this and subsequent error analyses, the 'best' solution was assumed to be the case where the number of elements in the x and y directions were set to 256. For this study, the average error (for data points from −20.0 mm to 20.0 mm) for each element number solution with respect to the 'best' solution with 256 elements was calculated and normalized relative to the peak to peak response of the best solution. Figure 2(b) presents the average normalized error with respect to varying element number from 2 to 128. With the plot scale set to Log_2 in the x direction and Log_{10} in the y direction, an essentially linear relationship between the scaled solution accuracy and scaled element number was found. This relationship is primarily associated with the increasing level of accuracy in representing a cylindrical hole using rectangular grid elements with smaller volumes of some partial conductivity at the hole boundary. Likewise, the phase response and associated error estimates in Figs. 3(a) and 3(b) respectively show similar convergence trends of reduced error with increasing element number. This relationship between average normalized error and element number can be defined by the following relation.

$$\log_{10}(\text{error}) = -m \cdot \log_2(N) + b. \tag{6}$$

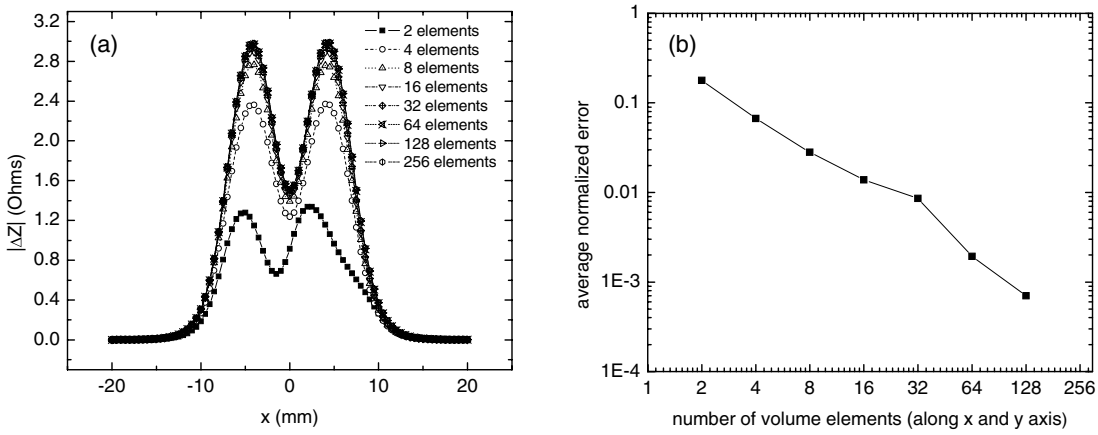

Fig. 2. Model convergence study varying the number of elements in the x and y directions for the case study problem plotting (a) the magnitude component of impedance and (b) the corresponding average normalized error with respect to the 256 element case.

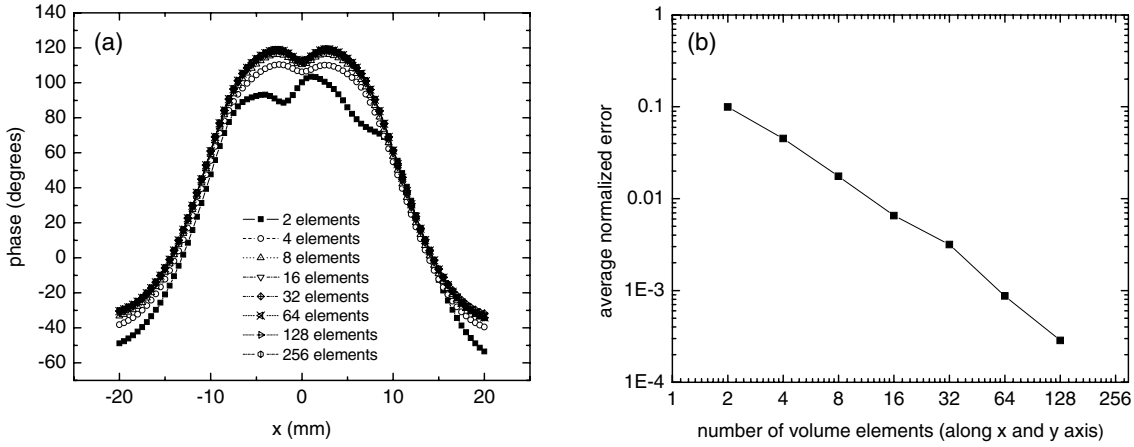

Fig. 3. Model convergence study varying the number of elements in the x and y directions for the case study problem plotting (a) the phase component of impedance and (b) the corresponding average normalized error with respect to the 256 element case.

An estimate of the exact solution can thus be found by extrapolating the exact solution as $N \to \infty$ by fitting the unknown parameters using a nonlinear least squares approach.

To investigate the ability of measurement models to accurately represent a crack around a fastener, convergence studies can also be focused to evaluate specific features associated with the presence of a crack. Since the hole is an axisymmetric feature while a radial crack extending from the hole is inherently asymmetric, a difference-based measure (about the axis of symmetry at $x = 0$) can be used to highlight changes in the measurement data associated with the non-asymmetric crack features. A straightforward difference calculation for the impedance data is defined as

$$dZ(x, y) = Z(x, y) - Z(-x, y). \tag{7}$$

Figure 4(a) displays the difference measure for the magnitude response as a function of x-axis scan position. Although the response does converge with increasing number of elements in the x and y directions, this feature associated with the crack response does not converge as previously with the dominant hole feature. To better study the nature of convergence, Fig. 4(b) presents the average normalized error with respect to varying element number from 2 to 128. Although there is a general trend toward

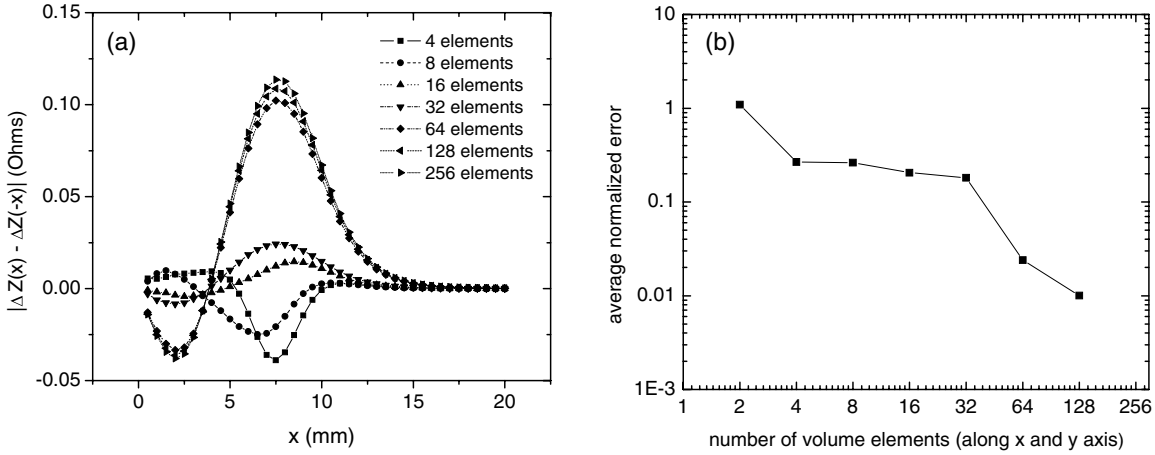

Fig. 4. Model convergence study varying the number of elements in the x and y directions for the case study problem plotting (a) the difference in the magnitude component of impedance (about $x = 0$) and (b) the corresponding average normalized error with respect to the 256 element case.

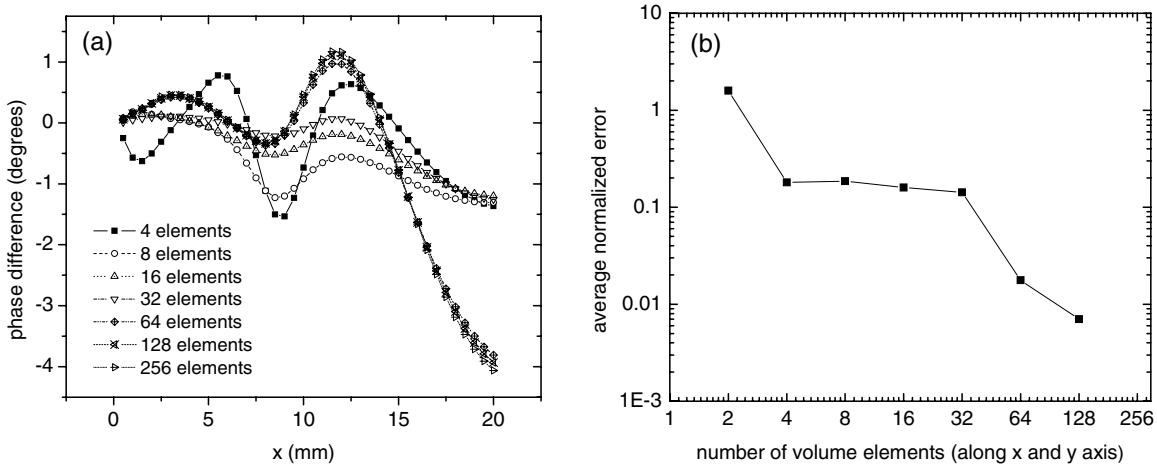

Fig. 5. Model convergence study varying the number of elements in the x and y directions for the case study problem plotting (a) the difference in the magnitude component of impedance (about $x = 0$) and (b) the corresponding average normalized error with respect to the 256 element case.

convergence, the most significant relative step improvement is found between 32 and 64 elements. Consider, the element width for 32 and 64 elements in the y-direction corresponds with 0.25 mm and 0.125 mm. In addition, the notch width of 0.25 mm was used in this study with the notch centered at $y = 0$. Thus, for the 32 element case, the notch is only represented by two elements in the y-direction that also extend into the aluminum layer, producing elements with partial conductivity and therefore not accurately modeling an open crack. However, for the 64 element case, two full elements with zero conductivity represent the notch width, accurately representing a fundamental characteristic of an open crack and properly forcing the flow of eddy currents around the notch. Thus, a minimum of 64 elements is required in the y direction to accurately represent the crack feature in the model. Likewise, the difference measure of the phase response and associated error estimates in Figs. 5(a) and 5(b) respectively show similar convergence trends with a significant reduction in error with 64 elements or more. This example demonstrates how convergence studies coupled with selective analysis of data features can be used to ensure that the key aspects of the model are accurately represented.

A second series of studies was performed varying the number of elements along the z axis from 2 to 16 by powers of 2. For x and y axis discretization, the number of elements was fixed at 64. The magnitude response and associated error estimates in Figs. 6(a) and 6(b) respectively show that the results do converge with increasing element number, but generally produce good results even with z equal to 2. As with the x and y axis convergence study, with the plot scale set to $\log_2$ in the x direction and $\log_{10}$ in the y direction, an essentially linear relationship between the scaled solution accuracy and scaled element number was found. Likewise, the difference magnitude response and associated error estimates in Figs. 7(a) and 7(b), respectively, show that the results do converge as well with increasing element number. Although the results also generally produce good results even with z equal to 2, there may be opportunities to refine the measurement model through an equation fit and extrapolation to evaluate the 'exact' solution.

3. TRANSFORMATION OF EXPERIMENTAL MEAUSREMENTS FOR MODEL COMPARISONS

3.1. Calibration-based Approach to Match Experimental and Model Data

In order to compare experimental and simulated data, it is necessary to evaluate the relationship between the output of the model with respect to experimental measurements. Harrison et al. proposed the use of an equivalent circuit model for an eddy current probe measurement and presented a procedure to quantify the parameters of the circuit using an impedance analyzer.[20–34] Fig. 8 shows a

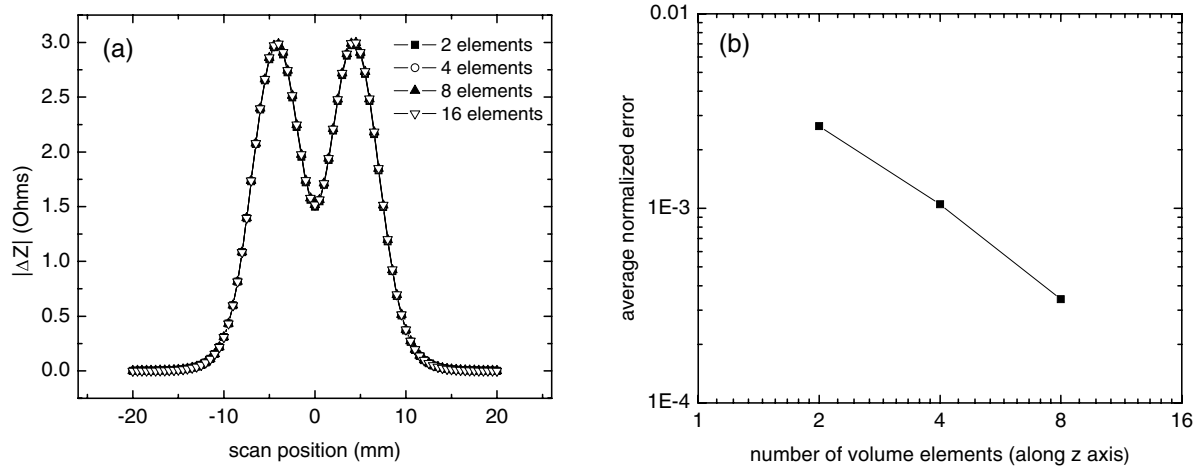

Fig. 6. Model convergence study varying the number of elements in the z direction for the case study problem plotting (a) magnitude component of impedance and (b) corresponding average normalized error with respect to 256 element case.

circuit diagram with an equivalent circuit model of the impedance measurement defined by Z_m. R_o and L_o are defined as the DC value for resistance and the low frequency inductance of the probe respectively, where the corresponding low frequency probe impedance, Z_o, is given by

$$Z_o = R_o + j\omega L_o. \tag{8}$$

The parallel impedance component, Z_p, is included to represent additional sources of impedance including the self-capacitance of the probe, cable resistance and lead capacitance. By this procedure, the impedance of the coil is first measured in air (Z_a) over a range of frequencies, and the DC values of resistance and inductance are then evaluated. Next, the parallel impedance component, Z_p, is calculated by evaluating the difference in admittance in air ($1/Z_a$) and the low frequency admittance ($1/Z_0$). Subsequent impedance measurements are required with the probe above the unflawed conductor, in order to relate the change in impedance measurements to the simulated change in impedance results due to the presence of a flaw region in a conductor.

Although this approach is quite appropriate for equating experimental and simulated data in the laboratory, there are several limitations when

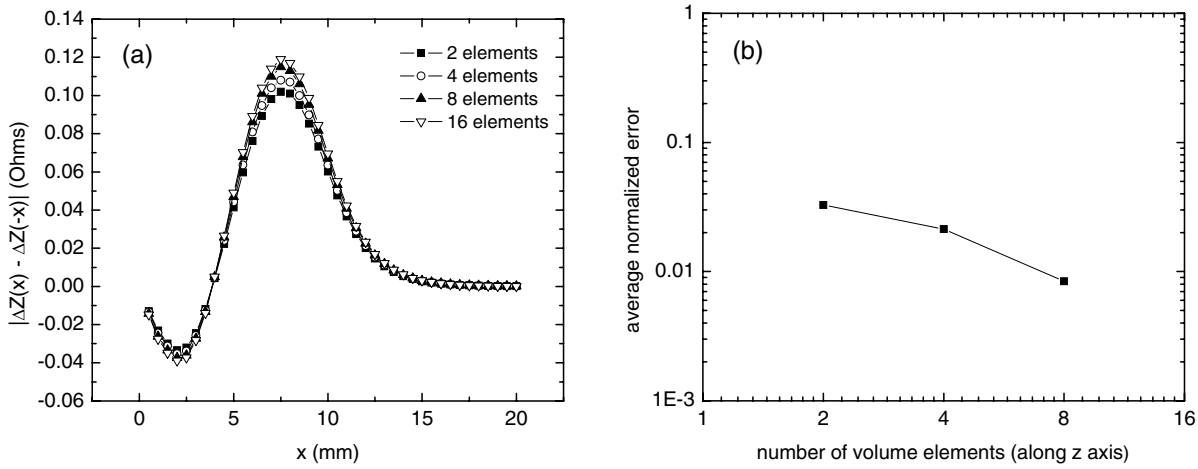

Fig. 7. Model convergence study varying the number of elements in the z direction for the case study problem plotting (a) the difference in the magnitude component of impedance (about $x = 0$) and (b) the corresponding average normalized error with respect to the 256 element case.

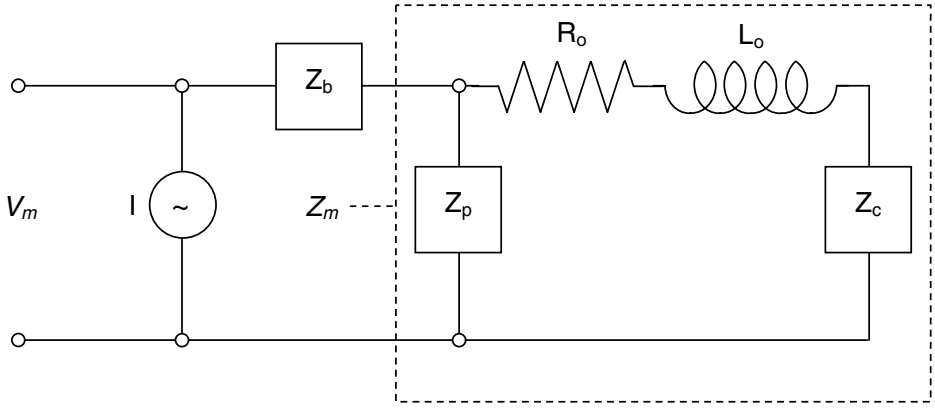

Fig. 8. Circuit diagram of eddy current inspections through impedance (Z_m) and voltage (V_m) measurements.

considering eddy current field inspections. First, this approach requires the use of an impedance analyzer. In practice, many automated eddy current systems acquire data through voltage-based measurements as shown in Fig. 10. In most cases, due to the additional equipment and labor costs, it is not desirable to include the use of an impedance analyzer in a practical inspection procedure. Second, it would also be beneficial to reduce the number of steps performed by the operator to evaluate this relation between model and experiment. A single measurement scan on a calibration sample in conjunction with a single transformation model adjustment would be most desirable. Lastly, to address the practical implementation of model-based classifiers such as inverse methods for voltage-based measurement systems, there is an additional need to accurately relate simulated impedance data with voltage measurements. Improvements in the reliability of inverse methods are expected if proper consideration is given to model accuracy through calibration.

An alternative approach is proposed for equating simulated impedance data and voltage-based measurements providing the basis for an in-service calibration procedure. Fig. 8 shows a circuit diagram expressing the relationship between measured

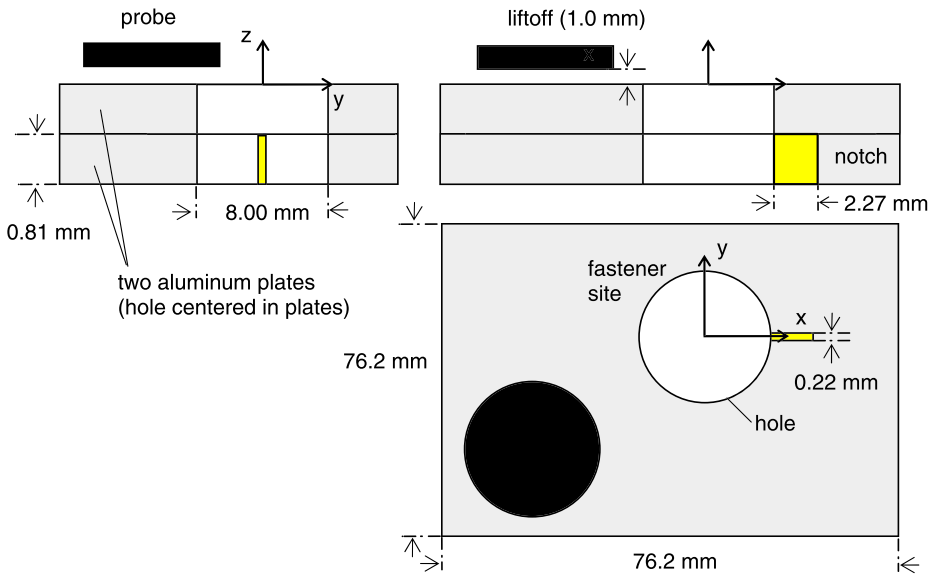

Fig. 9. A schematic diagram of the experimental setup of a two-layer fastener hole specimen with a subsurface notch.

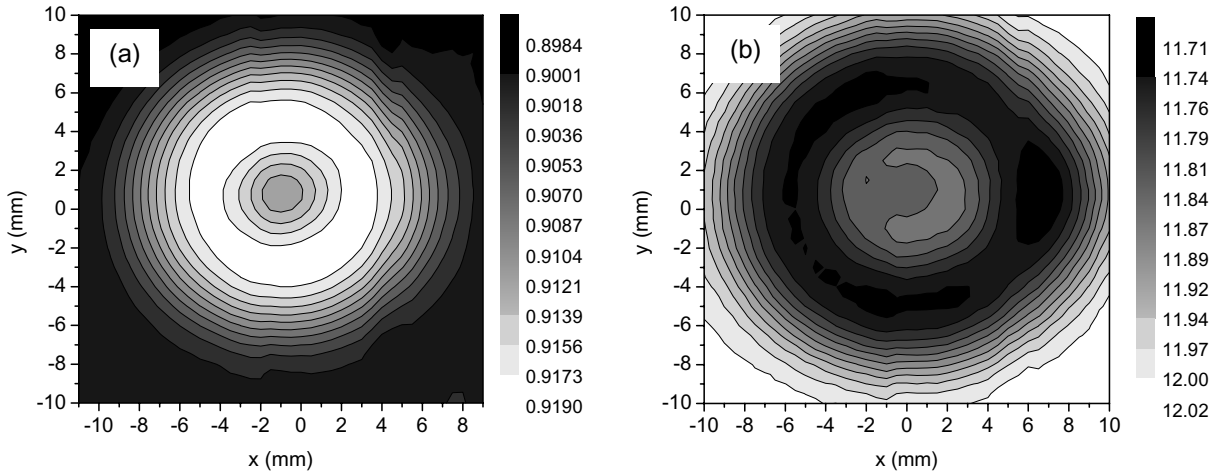

Fig. 10. Experimental data in voltage (a) magnitude and (b) phase.

voltage, V_m, and the equivalent coil impedance, Z_m, for an oscillatory current source, $I(f)$. Of particular interest is the relation between voltage measurements and the impedance due to the presence of a conductor, Z_c. The impedance due to a conductor can be subdivided into a constant impedance due to the un-flawed workpiece, Z_w, and a change in impedance term, ΔZ, associated with the presence of a flaw, ΔZ_f, and changes due to coherent noise, ΔZ_n, such that

$$Z_c = Z_w + \Delta Z = Z_w + \Delta Z_f + \Delta Z_n. \tag{9}$$

In particular, coherent measurement noise is associated with localized departures in the impedance of the workpiece due to non-flaw conditions such as probe lift-off, part geometry and material properties. Lastly, an additional bias impedance component, Z_b, is included in the model, to address any additional impedance producing an offset between the voltage and impedance measurements. Since most analytical and numerical models calculate the change in impedance due to a flaw in a workpiece, the relation between measured voltage, V_m, and change in impedance term, ΔZ, is of most interest. Simple circuit analysis yields the following relationship between the calculated change in impedance and the measured voltage:

$$V_m(\Delta Z) = IZ_b + \frac{IZ_p(Z_o + Z_w + \Delta Z)}{Z_p + Z_o + Z_w + \Delta Z}. \tag{10}$$

This equation can be written as:

$$V_m(\Delta Z) = a + \frac{b(\Delta Z + c)}{(\Delta Z + d)}. \tag{11}$$

where:

$$a = IZ_h$$
$$b = IZ_p$$
$$c = Z_o + Z_w$$
$$d = Z_p + Z_o + Z_w$$

Considering that each term is complex, resulting in a large number of parameters, it becomes difficult to accurately evaluate each unknown through a series of calibration runs. In addition, given the labor and difficulty of accurately estimating each electrical component separately, the use of approximate transformations are of interest. Linear models for transforming between voltage measurements and change in impedance have been proposed.[33,35] In practice, the approach of adjusting the magnitude and phase using calibration data from a reference flaw has been applied for improved flaw classification.[36] Radial basis neural networks models have also been proposed to equate model and measurement data while also including frequency and lift-off.[37] To better explore their practical viability, the theoretical justification for a linear transformation model will be presented in the next section.

3.2. Theoretical Basis for Approach Using Taylor Series Expansion

To explore the validity of a linear representation of the relationship between measurement voltage, V_m, and change in impedance, ΔZ, a Taylor series

expansion of the equivalent circuit model in Eq. (11) is used. A function, f, can be approximated using a Taylor series expansion,

$$f(x) = f(c) + f'(c)(x-c) + \frac{f''(c)}{2!} + (x-c)^2 + \frac{f'''(c)}{3!}(x-c)^3 \cdots + \frac{f^{(n)}(c)}{n!}(x-c)^n. \quad (12)$$

For this case, the Maclaurin series will be used with c set equal to zero. The series was evaluted to second order to both solve for the linear model and estimate the corresponding error term. The original function, V_m, and the corresponding first and second derivatives with ΔZ set equal to zero are given as follows:

$$f(0) = a + \frac{bc}{d}, \quad (13)$$

$$f'(0) = \frac{b(d-c)}{d^2}, \quad (14)$$

$$f''(0) = \frac{2b(d-c)}{d^3}. \quad (15)$$

The resulting linear model is given by

$$V_m(\Delta Z) = f(0) + f'(0)\Delta Z = a + \frac{bc}{d} + \frac{b(d-c)}{d^2}\Delta Z. \quad (16)$$

This equation can also be written in terms of two complex (four real) parameters representing a magntidue and phase adjustment with a bias correction in the impedance/measurement plane

$$V_m(\Delta Z) = (A + Bi) + (C + Di)\Delta Z. \quad (17)$$

This approach is proposed for general application. Two complex parameters can easily be evaluated through the use of calibration samples with known flaw sizes and corresponding model data that represent the range of expected flaws to be found. A least squares fit approach can be implemented with data taken over a range of flaw sizes and data samples for each flaw scan. In practice, a multi-point calibration approach is recommended, with a design dependent upon the sensitivity of the model parameters to the measurement.[38]

By expanding the equation to second order, an assessment of the error term can be made. The second order Taylor series expansion is given by:

$$V_m(\Delta Z) = a + \frac{bc}{d} + \frac{b(d-c)}{d^2}\Delta Z - \frac{2b(d-c)}{d^3}\Delta Z^2. \quad (18)$$

After replacing this term with the circuit components, the relation becomes:

$$V_m(\Delta Z) = IZ_b + \frac{IZ_p(Z_o + Z_w)}{(Z_p + Z_o + Z_w)} + \frac{IZ_p^2}{(Z_p + Z_o + Z_w)^2}\Delta Z - \frac{2IZ_p^3}{(Z_p + Z_o + Z_w)^3}\Delta Z^2. \quad (19)$$

Thus, a linear relationship exists between the measurement voltage and change in impedance as long as the change in impedance is small relative to the absolute impedance:

$$\left| \frac{Z_p}{Z_p + Z_o + Z_w}\Delta Z \right| \ll 1. \quad (20)$$

By definition, ΔZ is much smaller than Z_w. Also in general, Z_p is much smaller than $Z_p + Z_0 + Z_w$ for inspection measurements. From this Taylor series analysis, it can be concluded that this calibration-based approach is valid when the change in impedance due to a flaw condition is much smaller than the combined impedance of the baseline probe while in close proximity to the sample. It is also important to consider that this transformation is only appropriate if the inspection system frequency and probe characteristics are fixed. Separate calibration runs would be required for each test frequency and change of probe. Lastly, consideration must clearly be given to the resonance condition of the probe. Concerning the use of low frequencies (100 Hz −10 kHz) for crack detection around fastener holes, the effect of probe resonance is negligible. However, at higher frequencies where probe resonance becomes an issue, care must be taken toward applying this approach and consideration should be given to nonlinear voltage measurement transformations or the use of direct impedance measurements.

4. EXPERIMENTAL MODEL VALIDATION

4.1. Experimental Measurements for the Case Study Problem

The case study problem was designed to demonstrate the accuracy of the models. A diagram of the test samples is shown in Fig. 9. Two 2024-T3 aluminum plates with a conductivity of 18.76 MS/m were used. Each plate had a length, width, and height of 76.2 mm, 76.2 mm, and 0.81 mm respectively. The plates were in electrical contact during the experiment. A hole with a radius of 4.0 mm was drilled

through both of the plates. Finally, a notch with a width of 0.22 mm and a length of 2.27 mm was made in one of the plates. The inner and outer coil diameter measured 6.04 mm and 10.28 mm respectively. The height of the coil was 2.48 mm. The outer ferrite wall was 1.10 mm thick and the inner ferrite wall was 1.42 mm thick. The diameter of the hole inside the inner ferrite wall was 3.20 mm. With this setup, a 400 mm^2 area was scanned using a step size of 0.5 mm and a measured liftoff of 1.0 mm. The experimental data displayed in Fig. 10 were acquired using a lock-in amplifier that measured both the magnitude and phase of the voltage across the coil. The eddy current probe contains two coils manufactured by UniWest but only the coil nearest to the specimen was used for this experiment. The excitation for the coil was a 5.0 kHz sinusoidal signal. The amplifier discriminated the component of the received signal to measure the phase with respect to the excitation. The lock-in amplifier offered narrow band detection of the response from the coil at the reference frequency but rejected the noise signals that were very close to the reference frequency.[33]

Figure 10 displays images of the 2D raster scan voltage data acquired for the case study problem. A single line scan in the x-direction through the estimated center of the scan was extracted from the image data for use in calibration and comparison purposes. The four parameters, A, B, C, and D, associated with the transformation model (Eq. 17) were determined through the fitting of this experimental data feature vector with simulated data generated using VIC-3D®using a nonlinear least squares fitting routine found in Matlab. With this transformation, the experimental data can now be properly compared with simulated impedance data.

4.2. Model Validation Using Direct Comparisons

Validation of model results can also be addressed using a direct comparison with experimental data or simulated data generated using validated models. Comparisons between the experimental data, simulated data using the volume integral method and simulated data using the finite element method are presented for the magnitude and phase components of impedance in Figs. 11 and 12 respectively. Overall, there is very good overall agreement between the three data sets. This quality of the fit is somwhat expected since this same data set was used to calibrate the model with the

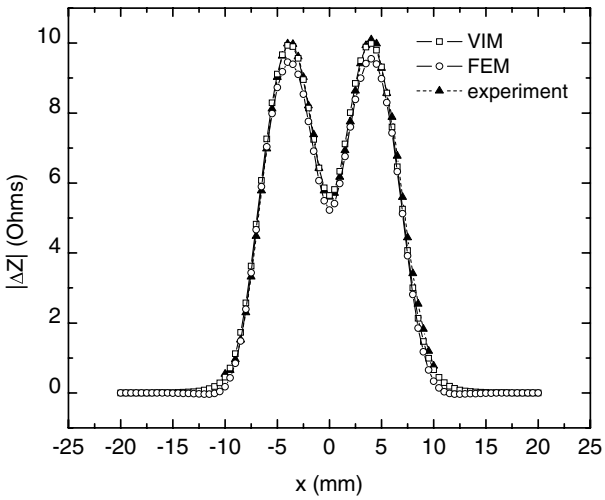

Fig. 11. Comparison of model and experimental data for the magnitude of impedance for the case study problem.

experimental data. However, due to the relatively small error between the data sets and similarity in shape that could not simply result from the four parameter fit, there is anecdotal evidence that the models can represent the experimental measurement. There is some discrepancy with the phase results as the probe is positioned far from the hole center, but this is somewhat artificial due to the very small values associated with the real and imaginary components resulting in the greater potential for error. Given the limited experimental data available, no absolute statements on the quality of model validation can be made. To properly validate both the

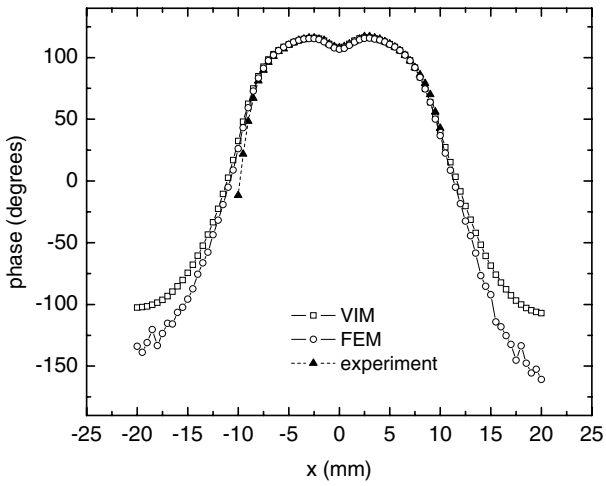

Fig. 12. Comparison of model and experimental data for the phase component of impedance for the case study problem.

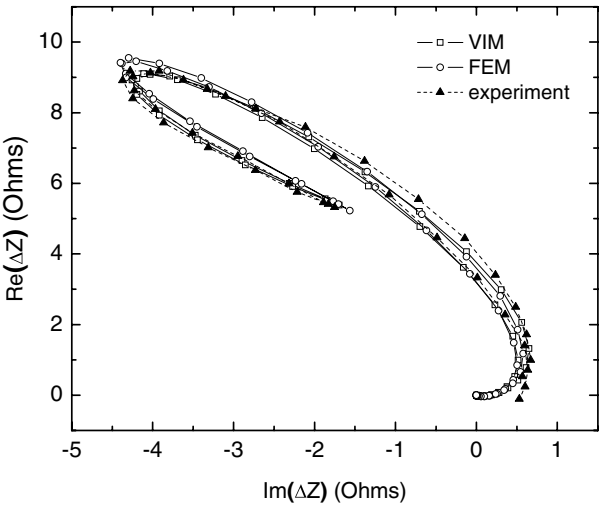

Fig. 13. Comparison of model and experimental data in the impedance plane for the case study problem.

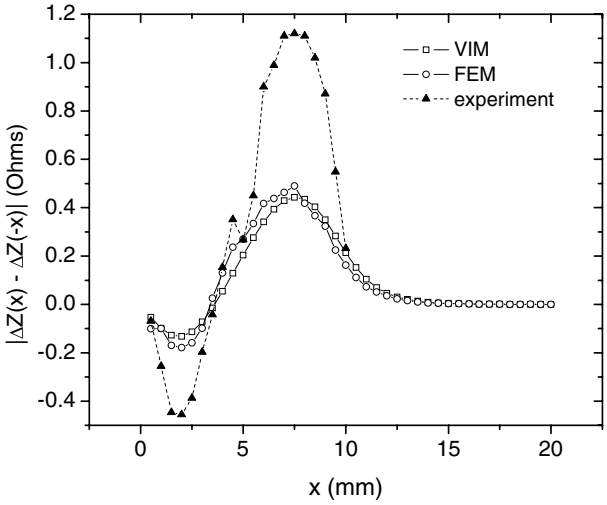

Fig. 14. Comparison of model and experimental data for the difference in the magnitude component of impedance highlighting the asymmetric response due to the presence of a notch.

model and model calibration method using experimental data, future work is planned to obtain and compare experimental data acquired under varying conditions such as hole diamater and flaw size.

In addition to magnitude comparisons, other characteristics of the measurement response can be used to qualify the model using experimental and validated model data. In particular, the characteristic shape of the curve should be in good agreeement. Figure 13 presents a comparison between the experimental and simulated data sets in the impedance plane. Given the characteristics of the linear transformation of the experimental voltage data to impedance, operations on the data in the impedance plane are in the form of translations $[A + Bi]$, rotations $[\tan^{-1}(D/C)]$ and amplification $[\sqrt{C^2 + D^2}]$. Thus, the characteristic shape of the response is not altered through the data transformation process. Qualitatively, there is very good agreement between the shape of the curves in Figs. 11–13. Deviations from a perfect match are likely due to imperfections in the probe model and noise in the experimental measurements. Internal asymmetries in the probe windings and slight differences in field response from the hole can contribute to these small differences. An error estimate across the entire feature vector can provide a good measure of the accuracy of the shape match.

The experimental data can also be preprocessed to highlight specific features associated with material characteristics of interest such as cracking. As in Section 2, difference measures are used to highlight the presence of an electron discharge machine (EDM) notch in the data. Figure 14 presents a comparison of model and experimental data for the difference in the magnitude of impedance highlighting the symmetric response due to the presence of a notch. First, there is very good agreement between the two models. In addition, the experimental data show very similar trends concerning locations of peaks and zero crossings, providing an indication that the general physics of the eddy current inspection technique is well represented by the models. However, there is an amplitude discrepancy between the experimental and simulated data by a factor of roughly 2.5. One potential source for the amplitude discrepancy is an inaccurate estimate of the hole center using the 2D raster scan data. The scan data were acquired with a step size of 0.50 mm in both the x and y directions. Due to the character of the difference calculation, small errors in the center estimate can produce errors in the magnitude of the difference results. A rudimentary

$$\text{error} = \sqrt{\frac{1}{N}\left\{\sum_{i=1}^{N}\left[\text{Re}\left(\Delta Z_{\text{exp},i}\right) - \text{Re}\left(\Delta Z_{\text{model},i}\right)\right]^2 + \left[\text{Im}\left(\Delta Z_{\text{exp},i}\right) - \text{Im}\left(\Delta Z_{\text{model},i}\right)\right]^2\right\}}, \tag{21}$$

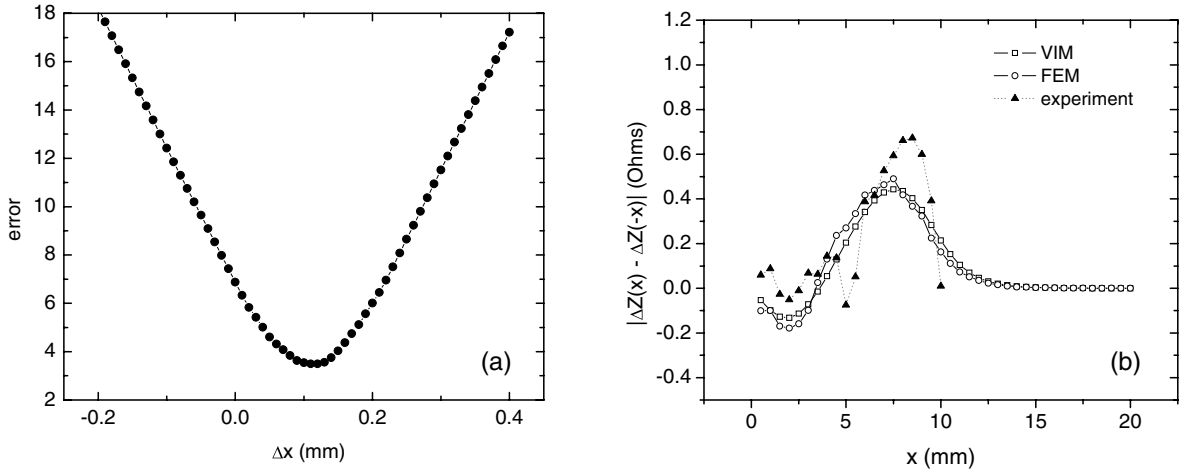

Fig. 15. Plots of (a) error between model and experimental data difference calculation as a function of varying center of experimental data using interpolation and (b) a comparison of model and experimental data for the difference in magnitude component of impedance with a center shift of $\Delta x = 0.12$ mm.

demonstration is presented in Fig. 15(a), where interpolation of the 1D feature vector in the x direction is performed and the accuracy of the model fit is estimated for varying the hole center. For this case, the optimum result for minimizing the error between the experimental and simulated data was found for the hole center shifted 0.12 mm. The corresponding data showing the match for the optimal case is shown in Fig. 15(b). The agreement in magnitude is generally much improved with this optimal shift in the hole center. Note that although the error minimization study between simulated and experimental data is not truly independent from the flaw response, since the hole response is significantly larger than the flaw response, the error fit is most sensitivity to matching the hole data and thus the hole center in this case. Unfortunately, the experimental data is not available to perform an independent evaluation of this assertion concerning hole centering being the main source of this error. However, anecdotal evidence indicates that it must be considered in future benchmark studies for this problem. An additional shift of the center in the y direction may also be the source of some of the remaining error, so ideally, 2D interpolation would greatly benefit any experimental based fit with models.

4.3. Model Validation Through Application As Inverse Method

Lastly, a particularly challenging task for models is demonstrating their capability to characterize the dimension of flaws such as crack length through inverse methods approaches. This has been one of the important research directions in quantitative nondestructive evaluation; however, difficulties remain due to the inherent ill-posed nature of most inversion problems and the inability of models to fully address the vast array of parameters requiring model inversion. A very basic demonstration of this concept is presented through estimation of a particular unknown parameter, probe liftoff, using inverse methods. Since liftoff is one of the most sensitive input parameters, multiple raster line scans across the flaw were simulated at several different liftoff values ranging from 0.05 to 1.85 mm. The root mean square error between the simulated and experimental data for multiple probe locations was calculated for each liftoff value using (21), and the results are displayed in Fig. 16. The least error occurs when the simulated liftoff was set to 1.00 mm which is equal to the measured liftoff value of 1.0 mm $\pm$0.1 mm. Although this is an example that is limited in scope, it successfully demonstrates an additional approach to validate the quality of models for future practical use.

5. CONCLUSIONS AND FUTURE WORK

Considerations in the use of convergence studies, validation with existing models, experimental validation studies and validation through inverse method demonstrations have been presented, exploring a continuum of methods to ensure the quality

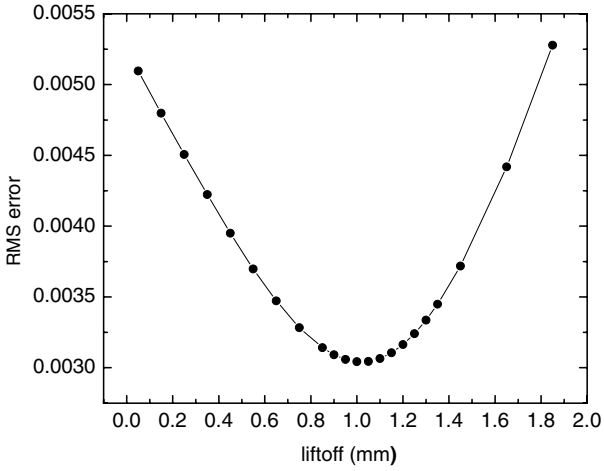

Fig. 16. RMS error between model and experimental data as a function of varying probe liftoff in the model.

of measurement models. A novel method of model calibration with experimental data has also been presented that will enable engineers in the NDE community to discover and make maximum use of NDE models. Through these studies, excellent agreement was generally found between the experiment and simulated studies, demonstrating the feasibility of using VIM and FEM to simulate the problem of detecting cracks around fastener holes.

Future work is foremost needed in the form of additional experimental data to fully validate the model. Independent experimental data is needed to appropriately validate the capability of transforming simulated data to represent voltage measurements. In addition, a series of studies exploring the limits of this model calibration approach in terms of varying probe lift-off, part material properties, hole geometry and flaw size are needed. Future work will also include using FEM and VIM to study magnetic field sensors such as the GMR and Hall effect sensors with the goal of optimizing the sensor size, and also the sensor position relative to the excitation source for improved sensitivity to radial cracks. With confidence in the modeling capabilities, parametric studies can now be conducted to identify potential features for classification. The complexity of the geometry of the problem will also be addressed in future work to include fastener heads, layer interfaces, and multiple defects in multiple layers. With simulation tools that address all key NDE measurement variables for this problem, research investigating optimum probe, sensor, and signal classification algorithm design for small crack detection and characterization is planned. Lastly, further demonstration of models in inverse method schemes to detect, locate and size fatigue cracks is proposed.

ACKNOWLEDGEMENTS

The authors would like to acknowledge support for this study provided by Air Force Office of Scientific Research. The authors thank Dr. Ray Ko of the University of Dayton Research Institute (UDRI) for support in the acquisition of experimental data, and Dr. Harold Sabbagh, Elias Sabbagh and Dr. R. Kim Murphy of Victor Technologies LLC for support with VIC 3D®.

REFERENCES

1. M. Bode and F. Spencer, Update of progress in the development of nondestructive inspection methods for detection of widespread fatigue damage, *ASNT Fall Conference*, (Pittsburgh, PA, 2003).
2. D. Hagemaier, B. Bates, and A. Steinberg, On-aircraft eddy current subsurface crack inspection, *Mater. Eval.* **46**, pp. 518–522 (1988).
3. T. Dogaru and S. T. Smith, Novel eddy current probes for detection of deep cracks around fastener holes, *Fifth Joint NASA/FAA/DoD Conference on Aging Aircraft*, (Orlando, FL, 2001).
4. D. Hayford and G. Kechter, Eddy current coils with spatially controlled field distributions, *Rev. Prog. Quant Nondest. Eval.* **10**, pp. 913–920 (1991).
5. R. Beissner, G. Burkhardt, E. Creek, and J. Fisher, *Rev. Prog. Quant. Nondest. Eval.* **12**, pp. 1017–1023 (1993).
6. M. Johnson, C. Lee, J. Henderkott, J. Knopp, and J. Aldrin, Conventional and pulsed eddy-current inspection utilizing hall-effect and induction coil detectors, AeroMat Conference, (Orlando Florida, 2005).
7. T. Dogaru and S. Smith, Giant magnetoresistance-based eddy-current sensor, *IEEE Trans. Magnetics* **37**(5), pp. 3831–3838 (2001).
8. R. Ko and M. Blodgett, Application of giant magnetoresistive (GMR) sensor for characterization of corrosion in a laboratory specimen, *Rev. Prog. Quant. Nondest. Eval.* **22**, pp. 844–851 (2003).
9. W. Avrin, Magnetoresistive eddy-current sensor for detecting deeply buried flaws, *Rev. Prog. Quant. Nondest. Eval.* **15**, pp. 1145–1150 (1996).
10. M. Gibbs and J. Campbell, Pulsed eddy current inspection of cracks under installed fasteners, *Mater. Eval.* **49**, pp. 51–59 (1991).
11. R. Rempt, Scanning with magnetoresistive sensors for subsurface corrosion, *Rev. Prog. Quant. Nondest. Eval.* **21**, pp. 1771–1778 (2002).
12. F. Thollon, B. Lebrun, N. Burais, and Y. Jayet, Numerical and experimental study of eddy current probes in ndt of structures with deep flaws, *NDT&E International* **28**(2), pp. 97–102 (1995).
13. B. Wincheski, J. Simpson, M. Namkung, D. Perey, E. Scales, and R. Louie, Development of giant magnetoresistive inspection system for detection of deep fatigue cracks under airframe

fasteners, *Rev. Prog. Quant. Nondest. Eval.* **21**, pp. 1007–1014 (2002).
14. N. Nakagawa, Theory of eddy current inspection of corner cracks, *Rev. Prog. Quant. Nondest. Eval.* **10**, pp. 249–254 (1991).
15. N. Nakagawa and J. Moulder, A model of bolt hole inspection via eddy current, *Rev. Prog. Quant. Nondest. Eval.* **12**, pp. 259–263 (1993).
16. Website, Model-Assisted POD Working Group, <www.cnde.iastate.edu/research/mapod>.
17. R. Beissner, K. Bartels, and J. Fisher, Prediction of probability of eddy current flaw detection, *Rev. Prog. Quant. Nondest. Eval.* **7**, pp. 1753–1760 (1988).
18. N. Nakagawa and R. Beissner, Probability of tight crack detection via eddy-current inspection, *Rev. Prog. Quant. Nondest. Eval.* **9**, pp. 893–899 (1990).
19. S. Rajesh, L. Udpa, and S. Udpa, Estimation of eddy current probability of detection (POD) using finite element method, *Rev. Prog. Quant. Nondest. Eval.* **12**, pp. 2365–2372 (1993).
20. D. Harrison, L. Jones, and S. Burke, Benchmark problems for defect size and shape determination in eddy-current nondestructive evaluation, *J. Nondestructive Eval.* **15**(1), pp. 21–34 (1996).
21. R. Murphy, H. Sabbagh, A. Chan, and E. Sabbagh, A volume integral code for electromagnetic nondestructive evaluation, Proceedings of the 13th Annual Review of Progress in Applied Computational Electromagnetics (Monterey, CA, March 1997).
22. J. Bowler, L. Sabbagh, and H. Sabbagh, A theoretical and computational model of eddy-current probes incorporating volume integral and conjugate gradient methods, *IEEE Trans. Magn.* **25**(3), pp. 2650–2664 (1989).
23. J. Bowler, L. Sabbagh, and H. Sabbagh, Eddy-current prove impedance due to a surface slot in a conductor, *IEEE Trans. Magn.* **26**(2), pp. 889–892 (1990).
24. J. Bowler, S. Jenkins, L. Sabbagh, and H. Sabbagh, Eddy-current probe impedance due to a volumetric flaw, *J. Appl. Phys.* **70**(3), pp. 1107–1114 (1991).
25. A. Raiche and J. Coggon, Analytic Green's tensors for integral equation modelling, *Geophys. J. R. Astr. Soc.* **42**, pp. 1035–1038 (1975).
26. T. Roberts, H. Sabbagh, and L. Sabbagh, Electromagnetic interactions with an anisotropic slab, *IEEE Trans. Magn.* **24**(6), pp. 3193–3200 (1988).
27. R. Beissner, Analytic Green's dyads for an electrically conducting half-space, *J. Appl. Phys.* **60**(3), pp. 855–858 (1986).
28. J. Bowler, Eddy Current Calculations using Half-Space Green's Functions, *J. Appl. Phys.* **61**(3), pp. 833–839 (1987).
29. R. Harrington, *Field Computation by Moment Methods*, Cazenovia, N.Y. (1968).
30. D. C. Carpenter, Use of the finite element method in simulation and visualization of electromagnetic nondestructive testing applications, *Mater. Eval.* **58**(7), pp. 877–881 (2000).
31. R. Palanisamy and W. Lord, Prediction of Eddy Current Probe Signal Trajectories, *IEEE Trans. Magn.* **16**(5), pp. 1083–1085 (1980).
32. Y. Tian, Y. Li, L. Udpa, and S. Udpa, Simulation for the world federation's first eddy current benchmark problem, *Rev. Prog. Quant. Nondest. Eval.* **23**, pp. 1560–1566 (2004).
33. J. S. Knopp, J. C. Aldrin, R. Ko, and H. Sabbagh, Numerical and experimental study of eddy current crack detection around fasteners in multi-layer structures, *Rev. Prog. Quant. Nondestr. Eval.* **23**, pp. 336–343 (2004).
34. H. A. Sabbagh, E. H. Sabbagh, R. K. Murphy, and J. Nyenhuis, Assessing thermal barrier coatings by eddy current inversion, *Mater. Eval.* **59**(11), pp. 21–34 (2001).
35. N. Nakagawa and B. P. C. Rao, Residual crack depth estimation in plates via frequency gradient measurement of EC impedance, *Rev. Prog. Quant. Nondest. Eval.* **24**, pp. 797–804 (2005).
36. L. Udpa, P. Ramuhalli, J. Benson, and S. Udpa, Automated analysis of eddy current signals in steam generator tube inspection, 16th World Conference on Nondestructive Evaluation, (Montreal, Canada, 2004).
37. N. Nakagawa and B. P. C. Rao, A study of boundary element eddy current model validation, *Rev. Prog. Quant. Nondest. Eval.* **24**, pp. 432–439 (2005).
38. W. D. Rummel, NDE procedure validation and use in NDE system calibration for NDE applications, *Rev. Prog. Quant. Nondest. Eval.* **24**, pp. 1982–1986 (2005).